WATER RESOURCES RESEARCH, VOL. 44, W08405, doi:10.1029/2007WR006179, 2008

Influence of fracture statistics on advective transport and implications for geologic repositories

Donald M. Reeves,[1] David A. Benson,[2] and Mark M. Meerschaert[3]

Received 17 May 2007; revised 21 February 2008; accepted 12 May 2008; published 2 August 2008.

[1] Large-scale (2.5 km by 2.5 km) simulations of fluid flow and solute transport through low-permeability fractured rock are assessed to determine suitability for hosting a nuclear waste repository. Multiple realizations of fracture networks with statistically realistic features are generated according to established methods. A novel continuum method provides a basis for solving flow and simulating particle trajectories through the fracture networks. Classical and fractional advection-dispersion models form the analytic foundation for statistical summaries of the transport of 25,000 conservative particles through the backbone of each network realization. Particle retention in low-velocity fractures, fast transport, and anomalous dispersion are all observed in the simulated plumes. Predictability is addressed by measuring the deviation of individual plumes from their ensemble average, taken over all realizations for each set of fracture network statistics. Fifteen sets of fracture network statistics are examined, ranging from dense networks of relatively short fractures to sparse networks of rather long fractures. Finally, the plume statistics are carefully examined in order to develop recommendations for suitable geologic repositories on the basis of fracture network statistics.

Citation: Reeves, D. M., D. A. Benson, and M. M. Meerschaert (2008), Influence of fracture statistics on advective transport and implications for geologic repositories, *Water Resour. Res.*, *44*, W08405, doi:10.1029/2007WR006179.

1. Introduction

[2] Proposals for the long-term disposal of high-level radioactive wastes emphasize the role of a geologic barrier in isolating these wastes from the biosphere. Upon release from a repository, the likelihood that a dissolved solute will travel to a distant receptor depends on the flow and transport properties of a fractured medium. The high degree of spatial variability in rock fracture properties, such as fracture length, density, permeability and network connectivity, results in highly heterogenous subsurface flow systems. Complexities associated with fluid flow and solute transport in fractured media have led to a reliance on highly detailed numerical models that explicitly represent individual fractures [e.g., *National Research Council*, 1996; *Neuman*, 2005; and references therein] for transport predictions. Site-specific numerical models depend on extensive field characterization efforts to collect physical and hydraulic data on deterministic structures.

[3] Analytical approximations that model transport as an advective-dispersive process may have advantages over numerical models that explicitly represent fracture networks, as quick and inexpensive screening-level solute transport approximations, constructed from limited field data. Analytical solutions also have the ability to describe solute transport at scales that exceed computational constraints of numerical models, with the possible exception of techniques that upscale transport according to "educated particles" whose motion is governed by transport statistics obtained from multiple, small-scale discrete fracture network simulations [e.g., *Schwartz and Smith*, 1988; *Painter and Cvetkovic*, 2005]. The accuracy of network-scale predictions based on advection-dispersion equations (ADEs) depends on fulfillment of the ergodic hypothesis: Have particles sampled enough of the heterogeneity in the system so that their statistical properties are essentially predictable? To address this important point, we consider classical and fractional ADE models as a framework for assessing ergodicity. We compare ensemble average plume shapes, combining all fracture network realizations for a given parameter set, to the point source solutions of these analytic ADE models. Then we use nonparametric statistical methods to measure the deviation of each individual plume, corresponding to one fracture network realization, from its corresponding ensemble average, as a way of assessing predictability.

[4] Advection-dispersion equations are closely connected with statistical limit theorems for normalized sums of independent and uncorrelated particle motions [*Bhattacharya and Gupta*, 1990; *Meerschaert and Scheffler*, 2001]. In this simplified setting, a cloud of particles will typically spread according to a multi-Gaussian elliptical contour, whose principal axes grow at the classical scaling rate of $t^{1/2}$ with time. For particles that travel through a fracture network, the motions are restricted to a small set of directions, which can violate the assumption of no correlation. However, in a dense fracture network consisting of relatively short fractures, the correlations may be insignificant, so that a multi-

[1]Desert Research Institute, Reno, Nevada, USA.
[2]Department of Geology and Geological Engineering, Colorado School of Mines, Golden, Colorado, USA.
[3]Department of Statistics and Probability, Michigan State University, East Lansing, Michigan, USA.

0043-1397/08/2007WR006179$09.00

Table 1. Properties of the Hydraulic Backbone

Set	a_1[a]	a_2	ρ_{2D}[b]	α[c]	γ_1[d]	γ_2[e]	t_{1km}[f]	$P(A)$[g]	$P(B\|A)$[h]	$P(AB)$[i]
1	1.0	1.0	0.015	1.0	0.48	0.9–1.0	1.00	2.3×10^{-3}	0.74	1.7×10^{-3}
2	1.0	1.0	0.035	1.0	0.42	0.9–1.0	0.46	1.2×10^{-2}	0.84	1.1×10^{-2}
3	1.3	1.0	0.013	1.1	0.35	1.0	2.15	1.1×10^{-3}	0.50	5.6×10^{-4}
4	1.0	1.6	0.17	1.2	0.27	0.9–1.1	1.00	2.4×10^{-3}	0.41	9.8×10^{-4}
5	1.3	1.9	0.16	1.4	0.23	0.9–1.1	10.0	1.2×10^{-2}	0.30	3.7×10^{-3}
6	1.6	2.2	0.22	1.5	0.19	0.9–1.1	4.64	2.7×10^{-2}	0.20	5.4×10^{-3}
7	1.9	1.9	0.20	1.5	0.23	0.9–1.0	100.0	3.3×10^{-2}	0.23	7.4×10^{-3}
8	1.9	1.9	0.20	1.5	0.20	1.0	100.0	2.3×10^{-2}	0.18	4.2×10^{-3}
9	1.9	2.2	0.35	1.5	0.60/0.18	1.0	46.4	1.9×10^{-1}	0.79	1.5×10^{-1}
10	1.9	2.5	0.33	1.6	0.28/0.14	0.9–1.2	100.0	8.9×10^{-2}	0.33	3.0×10^{-2}
11	2.5	2.8	0.27	1.7	0.14	1.0–1.2	2154	4.7×10^{-2}	1.7×10^{-2}	8.1×10^{-4}
12	2.5	2.8	0.48	1.5	0.95/0.16	exp(-z)	464.2	3.4×10^{-1}	0.91	3.1×10^{-1}
13	2.8	3.0	0.30	1.7	0.12	0.9–1.0	10,000	3.7×10^{-2}	6.7×10^{-4}	2.5×10^{-5}
14	2.8	3.0	0.40	1.5	0.95/0.17	exp(-z)	464.2	3.7×10^{-1}	0.92	3.4×10^{-1}
15	3.0	2.8	0.50	1.5	0.50/0.33	1.0–1.2	464.2	2.5×10^{-1}	0.67	1.7×10^{-1}

[a]Power law fracture length exponent.
[b]Average spatial fracture density value in model domain (m/m^2).
[c]Spreading-rate exponent along primary plume growth direction.
[d]Power law decay of particles remaining in source area.
[e]Power law decay of $1/v$.
[f]Time of first solute particle "slug" reaching a transport distance of 1 km (years).
[g]Probability of a solute particle entering hydraulic backbone.
[h]Probability of a solute particle in hydraulic backbone traveling $\geq$ 1 km in 10^4 years.
[i]Conditional probability of a solute particle both entering the hydraulic backbone and traveling $\geq$1 km in 10^4 years.

Gaussian plume can emerge. An alternative fractional ADE for vector jumps employs a fractional derivative in place of the usual second derivative, or Laplacian, in space [*Meerschaert et al.*, 2001; *Schumer et al.*, 2003a]. This model pertains when the particle motions are heavy tailed, with a jump length probability that falls off like a power law. Since fracture statistics (length and transmissivity) are power law, it is reasonable to explore these alternative models. The point source solutions to the fractional ADE in multiple dimensions are called operator-stable densities [*Jurek and Mason*, 1993; *Meerschaert and Scheffler*, 2001; *Schumer et al.*, 2003a]. They provide an alternative analytic model for particle plumes representing an accumulation of temporally uncorrelated heavy tailed jumps. The parameters defining an operator-stable density include the primary growth coordinates, which need not be perpendicular, and a power law growth index for each coordinate. For the multi-Gaussian, actually a special case of the operator stables, the primary growth directions are the principal axes of the ellipse. However, the shape of an operator-stable plume can also be strongly nonelliptical.

[5] *Reeves et al.* [2008a, 2008b] reported a detailed simulation study that forms the basis for this work. Fifteen parameters sets, representing a range of realistic fracture statistics, were studied. For each set, 500 realizations of a fracture network were simulated. For each realization, a novel fracture continuum approach was used to solve for the flow field over the 2.5 km by 2.5 km domain, and a standard particle-tracking code was employed to trace 25,000 particles in advective motion starting in a 100 m by 100 m source release area. Ensemble plumes, taken over all realizations of the fracture network for a given parameter set, were found to closely resemble operator-stable or multi-Gaussian shapes. Analysis of ensemble plumes suggests that measurable statistical properties of the fracture networks, particularly the distribution of fracture length and values of fracture density, can be used for ADE model selection (classical versus fractional) and ADE parameter estimation. The multiscaling fractional-order ADE requires only a few more parameters than the classical ADE, specifically the principal scaling directions and rates of plume growth [*Meerschaert et al.*, 2001; *Schumer et al.*, 2003a; *Reeves et al.*, 2008b].

[6] Ensemble plumes produced from sparsely to moderately fractured networks with relatively long fractures (sets 1–9, Table 1) reflect many characteristics of operator-stable densities including power law tails, super-Fickian plume growth rates (plume spreads faster than $t^{1/2}$), different growth rates in each coordinate corresponding to fracture orientations, and nonelliptical shape with distinct multidimensional skewness (Figure 1). Ensemble solute transport through moderately to densely fractured networks with relatively short fractures (sets 10–15, Table 1) resulted in elliptical plumes resembling multi-Gaussian densities (Figure 9).

[7] In addition to an analysis of deviations between ensemble plumes and individual realizations to assess the degree that plumes are ergodic (predictable), a probabilistic framework based on advective particle transport is adopted to recommend fracture statistics of low-permeability rock masses that are most suitable for the disposal of high-level radioactive waste. For this characterization, properties of the hydraulic backbone are evaluated, including (1) the probability that a solute particle will enter the hydraulic backbone, (2) the probability that solute particles undergo large net transport distances $\geq$1 km, (3) the propensity for fast particle transport, and (4) the statistical nature of particle retention. The organization of this paper reflects these objectives by describing, for each hypothetical fracture network parameter set, transport statistics of particle plumes traveling through the hydraulic backbone, and quantification of realization-to-realization plume variability. Finally, we summarize those results, to identify the sets of realistic fracture network

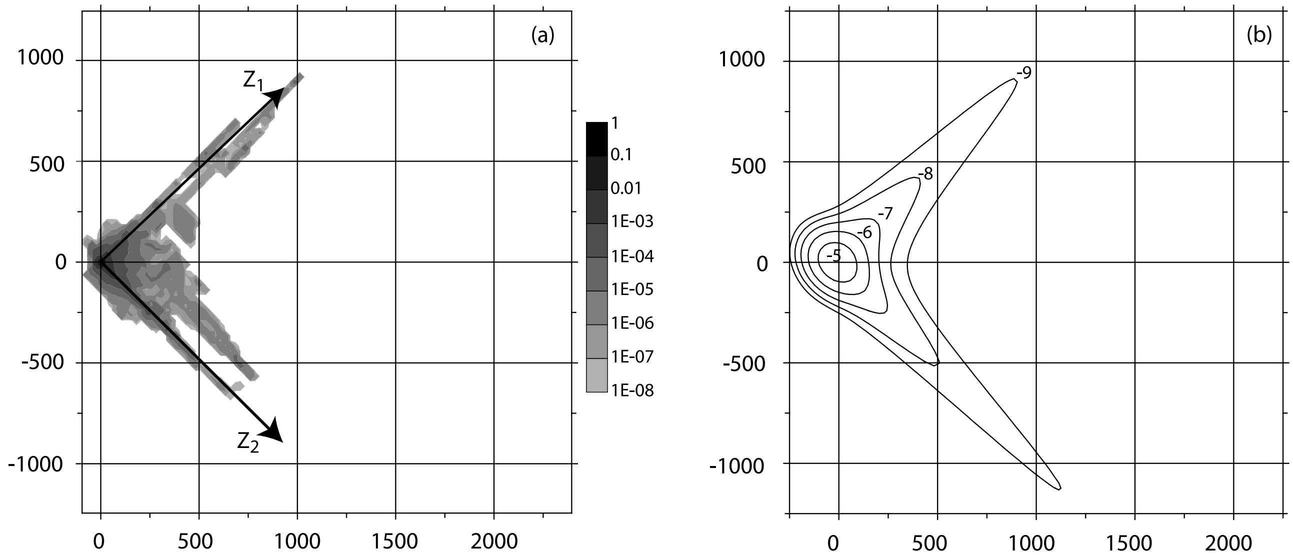

Figure 1. (a) Ensemble particle displacement plume for set 8 statistics (Table 1) exhibits several characteristics of (b) an operator-stable density including power law leading plume edges (not shown) and super-Fickian plume growth rates along primary plume growth directions (denoted Z_1 and Z_2). Though growth rates in Figure 1b are equal ($\alpha = 1.9$), asymmetry in the operator-stable density reflects a higher probability for particle transport in the fracture group with greater fracture density (oriented at $-45°$). Concentration levels in Figure 1b are powers of 10. All spatial values are in units of meters.

statistics most suitable for a geologic repository in low-permeability fractured rock.

2. Numerical Simulations of Flow and Transport

[8] We present a brief summary of the numerical simulations here; see *Reeves et al.* [2008a] for details. The large-scale (2.5 km by 2.5 km) fluid flow and solute transport simulations provide synthetic data used for these analyses. A total of 15 parameter sets, defined as a group of values used to assign fracture length, density, and orientation, represent a wide variety of fracture network types (Table 1). Five hundred equiprobable fluid flow and solute transport realizations were generated for each parameter set. Ensemble plumes were constructed from all individual realizations of a parameter set (e.g., Figure 1a).

[9] A Pareto distribution, $P(Y > y) = wy^{-a}$, was used to control fracture trace lengths (above a certain cutoff) by allowing the value of the power law exponent, a, to vary between 1 and 3 [*Davy*, 1993; *Renshaw*, 1999; *Bonnet et al.*, 2001]. In general, sample mean fracture length decreases as a increases. The distributional properties of fracture transmissivity and placement (or spacing) were the same for all parameter sets. Transmissivity values assigned to individual fractures were heavy tailed on the basis of an upper truncated Pareto distribution where values were allowed to range from 10^{-11} to 10^{-2} m^2/s according to a power law exponent of 0.4 [*Gustafson and Fransson*, 2005; *Kozubowski et al.*, 2008]. Fracture length and transmissivity were assumed uncorrelated in the simulations. Fracture centers were uniformly scattered across the model domain, resulting in a spatial Poisson point process with exponential spacing between fractures [*Ross*, 1985; *Rives et al.*, 1992; *Brooks et al.*, 1996; *Wines and Lilly*, 2002]. Fractures were placed into the model domain until a specified spatial density (ρ_{2D} [m/m^2]), defined by the sum of fracture lengths per unit area, was reached. For the simulated networks, values of spatial density required to reach the percolation threshold increase with increasing values of a. This is related to the decrease in typical fracture length as a increase from 1 to 3. A positive correlation between fracture density and the power law index a was observed in natural fracture networks by *Renshaw* [1997, 1999], which may be related to the role of fluid pressure during fracture propagation. If fluid pressure is a driving force behind fracture propagation, the release of excess fluid pressure at the percolation threshold may cause fracturing to cease [*Renshaw*, 1996].

[10] Using a novel continuum algorithm [*Reeves et al.*, 2008a], the fracture networks were translated onto a finite difference grid of equal cell size (1 m by 1 m by 1 m) and MODFLOW [*McDonald and Harbaugh*, 1988] was used to solve for fluid flow, in both the fracture network and the less permeable matrix. To restrict the transport of solutes to fractures, a matrix transmissivity of 10^{-15} m^2/s was assigned to cells not occupied by fractures. This resulted in, essentially, solution of a discrete network, which is a set of linear equations of pressures at intersections. MODFLOW solves a similar set along entire fractures and also allows for detailed modeling of fracture/matrix interaction by increasing matrix transmissivity. All model domain boundaries are constant head, inducing mean fluid flow from left to right according to a linear hydraulic gradient of 0.01. The boundary configuration represents an unbounded fractured rock mass where both fluid and solutes can exit any down-gradient boundary. Random walk particle method for simulating transport in heterogeneous permeable media (RWHet) (E. M. LaBolle, RWHet: Random walk particle model for simulating transport in heterogeneous permeable media, version 2.0 user's manual and program documentation, 2000) was used to simulate trajectories of conservative

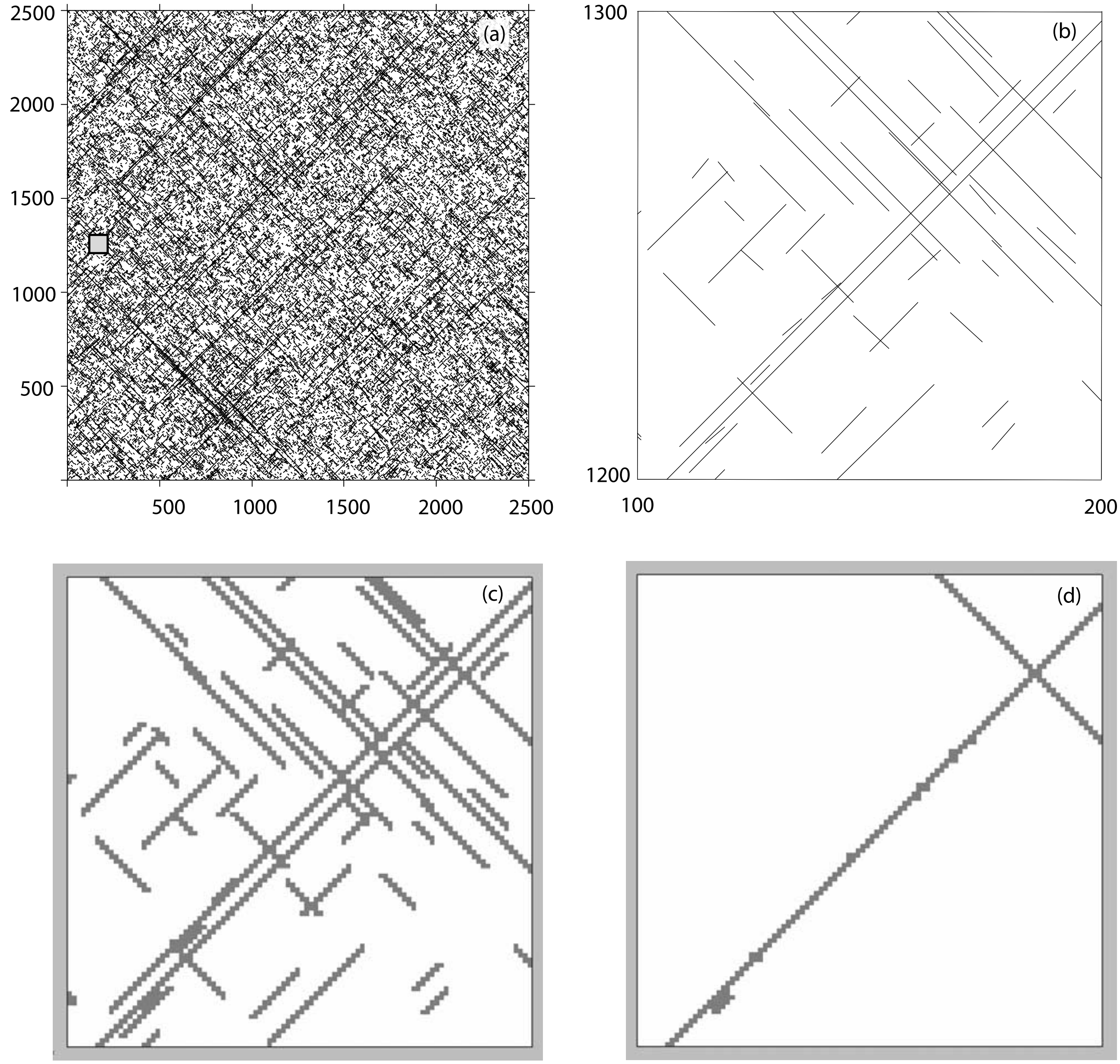

Figure 2. (a) Fracture network realization consisting of two fracture sets oriented at ±45° with length exponent values of 1.5 with (b) subsection of domain subject to particle release corresponding to shaded area in Figure 2a, (c) finite difference grid representation of Figure 2b, and (d) cells representing hydraulic backbone within source release area. Other fractures within source release area not included in Figure 2d are either isolated from the hydraulic backbone or do not meet the Darcy cell velocity criterion (e.g., dead-end segments). Spatial dimensions of the network are in meters.

solute particles through the fracture networks as an advective process. Diffusion into the matrix was excluded from these simulations, since our main goal was to study the leading plume edge. Particles travel through individual fractures as individual piston flow slugs with a small amount of numerical (within-fracture) dispersion that varies according to fracture orientation. Values of within-fracture dispersivity are less than 1/1000 of the scale of transport indicating that numerical dispersion does not influence overall solute transport behavior [*Reeves et al.*, 2008a].

[11] To mimic a geologic repository where the release of contaminants over a large spatial area is possible, 25,000 particles were placed into a 100 m by 100 m box that extends from 100 m to 200 m in the *x* direction and 1200 m to 1300 m in the *y* direction (Figure 2). The hydraulic backbone of each network realization was not defined prior to mapping onto the finite difference grid. Instead, we allowed MODFLOW to solve the Darcy flow equation in all fracture segments. Only cells corresponding to interconnected fracture segments of the backbone contain values of Darcy cell velocity significantly greater than the background matrix (Figure 2). Solute particles were released only into these "backbone" cells within the release area. The Darcy cell velocity criteria was not the same for all parameter sets.

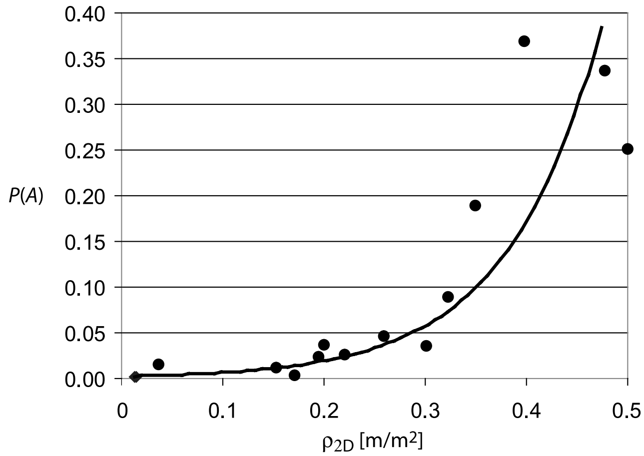

Figure 3. Influence of spatial density (ρ_{2D}) on the probability of a solute particle entering the hydraulic backbone, $P(A)$. Note that spatial density is defined as the sum of fracture lengths normalized by the area of the domain. Values of $P(A)$ increase with density in a nonlinear trend. A best fit exponential trend line is presented for comparison.

Preliminary simulations (sets 5, 8–10, and 13–14) used a Darcy cell velocity cutoff of 2 orders of magnitude greater than the average matrix value to define a hydraulic backbone. For all other subsequent simulations, the Darcy cell velocity cutoff was increased to 3 orders of magnitude to minimize particle retention in less transmissive fractures. Particle displacements were recorded for 16 equally spaced log cycle time increments that spanned 5 orders of magnitude.

3. Properties of the Hydraulic Backbone

[12] The likelihood of a solute particle leaving a fractured rock mass and entering the biosphere depends on the properties of the hydraulic backbone, a subset of interconnected fractures that is responsible for preferential fluid flow and solute transport within a rock mass. Conservative solute particles are released into all fractures of the hydraulic backbone within the release area. The probability that a contaminant particle will reach the biosphere depends on two events: (1) a particle in the release area must encounter a fracture on the backbone and (2) once in the backbone, the particle must move a significant distance (1 km here). A sparse network with longer fractures may have a low probability that backbone fractures are present in the source area, but once a particle enters the backbone, the probability is high that the particle will travel large distances. The probability that a particle enters the biosphere is the product of these two probabilities, which we estimate from the particle-tracking simulations.

3.1. Probability of Entering the Hydraulic Backbone

[13] The probability of a contaminant entering the hydraulic backbone is quantified by simply counting the number of backbone cells in the particle release area. Particles are subsequently released uniformly into these cells (the source is not flux weighted). A more complex initial condition might allow the particles to diffuse within the rock matrix toward the active fractures [e.g., *Berkowitz and Scher*, 1996]. Not all realizations contain cells on the hydraulic backbone in the particle release area; hence, transport does not occur in these realizations. On the basis of a total of 500 network realizations per parameter set, the number of realizations that contribute to transport (contain at least one backbone cell in the release area) range between 189 to 500. To compute the probability of the event "A", defined as a solute particle entering the hydraulic backbone, the total number of backbone cells for each parameter set is computed and normalized by the total number of cells in the release area. Note that the computation of $P(A)$ includes all 500 realizations of a parameter set regardless of contribution to transport.

[14] Values of $P(A)$ are low ($\leq$25%) for all simulations indicating that only a small subset of cells in the particle release area (even for very dense networks) are on the hydraulic backbone (Table 1). The probability of a particle entering a backbone cell is primarily controlled by values of spatial fracture density (Figure 3). Note that spatial density values, defined as the sum of fracture lengths normalized by the area of the domain, are correlated with the distribution of fracture length in our simulations. Networks with longer fractures reach the percolation threshold at lower densities, and conversely, networks with shorter fractures require much higher densities to percolate. As a general trend, the lowest probabilities (on the order of 10^{-3}) correspond to sparse networks containing very long fracture lengths (sets 1, and 3–4) and the highest probabilities (on the order of 10^{-1}) correspond to very dense networks with short fracture lengths (sets 9, 12, and 14–15) (Figure 3). Note that the density used in set 2 (second point from left in Figure 3) is artificially high (well above percolation) for the fracture length distribution. This network had a probability roughly 10 times that of similar networks. If $P(A)$ was the only criterion for repository selection, the sparsest networks with fewer, longer fractures would be preferred.

3.2. Transport of Conservative Particles

[15] After the backbone cells are counted in the source area, we uniformly place 25,000 particles in those cells, and track their net displacement using a standard particle-tracking code (RWHet). We then calculate the conditional probability of event "B" defined as a particle displacement $\geq$1 km, given that the particle has entered the backbone in the source area. A net vector displacement of 1 km is used to define particles that undergo large net transport distances, since the simulated fracture sets possess multiple configurations of orientation. This measured probability, $P(B|A)$, is the likelihood that a solute particle will be transported over a large distance within the same time period (10,000 years) that was used previously for performance assessments of the Yucca Mountain proposed repository [*Ewing et al.*, 1999]. Rather than emphasizing fast or slow particle transport which may only affect a small subset of ensemble solute particles, the use of this statistic evaluates the potential that any particle of an ensemble plume undergoes large displacement. Note that only conservative transport is considered; inclusion of reactive transport processes and radioactive decay would reduce $P(B|A)$.

[16] A clear trend between values of $P(B|A)$ and fracture network statistics is not apparent (Table 1 and Figure 4). Generally, $P(B|A)$ is high and on the order of 10^{-1}, indicating that, within percolating networks, it is likely that

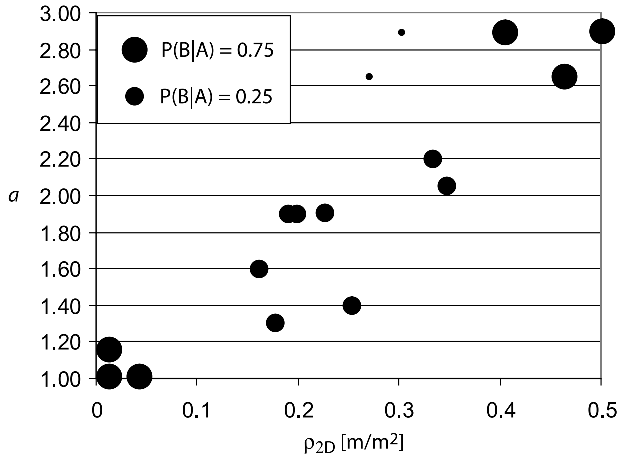

Figure 4. The influence of mean fracture length exponent (a) and spatial density (ρ_{2D}) on the probability of a solute particle traveling at least 1 km in 10,000 years ($P(B|A)$). The size of the dot is proportional to the value of $P(B|A)$.

a solute particle will travel a long transport distance if introduced into a segment of the hydraulic backbone. The highest values ($P(B|A) > 0.70$) occur for sets 1 and 2 (sparse domains with very long fractures) and sets 12 and 14 (very dense networks with very short fractures) (Figure 4). A high value (0.79) also occurs for set 9 (very dense domain with intermediate fracture lengths). Though set 15 ($P(B|A)$ = 0.67) describes networks similar to sets 12 and 14, the lower value of $P(B|A)$ may be explained by fracture set orientation. Unlike the ensemble plumes for sets 12 and 14, fracture set orientations for set 15 (θ_1 = 30°, θ_2 = 10°) produce an ensemble plume (not presented) that is not aligned in the direction of the hydraulic gradient causing slower particle migration rates. The lowest $P(B|A)$ values occur for sets 11 and 13 which have probabilities on the order 10^{-4} and 10^{-2}, respectively (Figure 4). These parameter sets describe networks that are dominated by very short fractures at densities that are just above the percolation threshold. As reflected in the t_{1km} statistic (Table 1), the combination of spatial density values near the percolation threshold and very short fracture lengths enhances plume spreading transverse to the hydraulic gradient, and consequently, reduce particle migration rates.

[17] Once a solute particle is introduced into the hydraulic backbone, the probability that it leaves a fractured rock mass and enters the biosphere is controlled by transport properties of the network. *Reeves et al.* [2008b] computed estimates of the scaling exponent (α) for all networks (sets 1–15) according to [*Benson et al.*, 2000; *Schumer et al.*, 2003a]:

$$\sigma \propto t^{1/\alpha} \tag{1}$$

where σ is an empirical measure of plume size and α governs the rate of spreading (Table 1). For dense networks of shorter fractures ($a \geq 2$), ensemble particle plumes follow elliptical contours whose principal axes are orthogonal, and weakly aligned with fracture set orientations. For these plumes (sets 10–15), values of α in Table 1 represent the rate of growth along the longitudinal plume axis, and reflect our interest in early breakthroughs. Fickian growth (α = 2) was typically observed along the transverse axis in these networks of shorter, denser fractures [*Reeves et al.*, 2008b].

[18] Sparse fracture networks with long fractures ($a < 2$) produce ensemble plumes that exhibit super-Fickian growth rates ($\alpha < 2$) (Figure 1a). These plumes have unique rates of spreading (α_1, α_2) along each primary growth direction that contribute to the leading plume edge. Since the spreading of a solute plume along a principal growth direction is proportional to t^{1/α_i}, lower values of α_i correspond to faster plume growth rates. We average the two values of α_i into a single metric, α, that is used in a latter section to evaluate the propensity for rapid early time breakthroughs (Table 1). Note that the averaging of α_1 and α_2 only occurs for nonelliptical plumes resembling operator-stable densities (sets 1–9).

[19] Super-Fickian transport rates were observed for all ensemble plumes resembling multi-Gaussian densities (Table 1). We attribute this to particle retention in low-velocity fractures near the source area [*Berkowitz and Scher*, 1997]. It is interesting that the multi-Gaussian plume shapes correspond to fracture length exponents $a \geq 2.0$, since this is also the theoretical cutoff for multi-Gaussian central limit theorem behavior [*Meerschaert and Scheffler*, 2001].

3.2.1. Fast Particle Transport

[20] Values of the spreading rates α are similar for several of sets 1–5, and do not necessarily reflect transport times of the fastest particles over a specified distance (Figure 5). Travel time of the fastest particle out of an ensemble to reach a net radial distance of 1 km, t_{1km} (years) is computed as an additional metric of fast particle transport (Table 1). Though these times are based on the fastest particle, the combination of releasing 25,000 particles into a much smaller subset of backbone cells within the release area (as demonstrated by values of $P(A)$) and minimal within-fracture dispersion [*Reeves et al.*, 2008a]) causes particles to migrate as near piston flow "slugs" through individual fractures. Essentially, values of t_{1km} describe the fastest slug of particles out of a total of 500 individual realizations. Note that t_{1km} values are constrained to logarithmic time steps. Though values of t_{1km} provide sufficient information on fast particle transport for comparisons of our networks, a finer level of discretization in time would yield more precise values.

[21] Transport times based on the t_{1km} metric demonstrate that both the distribution of fracture lengths (as denoted by a_i) and density control fast solute particle motion. Times for particle slugs to reach a displacement of 1 km range from only 0.46 years for set 2 (a_1 = 1.0, a_2 = 1.0) to 10,000 years for set 13 (a_1 = 2.8, a_2 = 3.0). When fracture lengths are equal (sets 1–2, 11–12, and 13–14), higher-density values decrease transport times. For sparse networks containing relatively long fractures (sets 1 and 2), the contrast in transport times is related to the increase in likelihood that long fractures with high velocities will intersect the particle release area. For networks comprising shorter fractures (sets 11 and 12 and sets 13 and 14), the influence of spatial density on transport time is related to flow path tortuosity. Fewer flow paths are available to solute particles at lower densities, causing a higher degree of solute spreading transverse to the hydraulic gradient. As spreading transverse

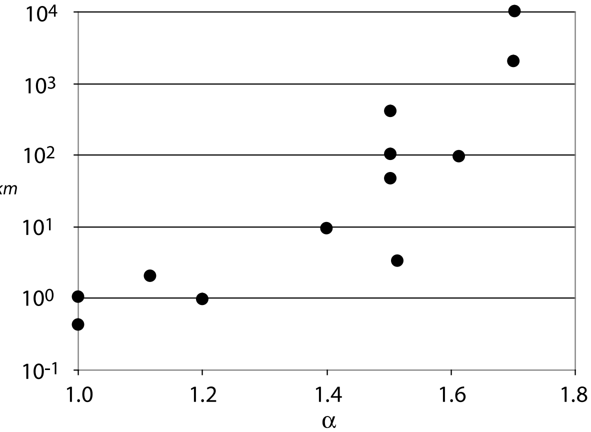

Figure 5. A weak positive relation exists between the time that it takes for the fastest particle slug to reach a radial distance of 1 km (t_{1km}) and the mean value of α, a measure of the rate of plume growth.

to the gradient increases, t_{1km} transport times increase. Lower values of spatial density in set 11 result in a t_{1km} of 2154 years, while a 0.21 m/m^2 (44%) increase in density decreases t_{1km} to 464 years for set 12. A 0.10 m/m^2 increase in density (25%) from the value used in set 13 decreases transport times in set 14 by nearly 2 orders of magnitude (10,000 to 464 years).

3.2.2. Particle Retention

[22] A large portion of solute mass remains in, or near, the source release area for the majority of individual plume realizations and all ensemble realizations, regardless of network type. Velocities of independent particle trajectories demonstrate that slow particles are not erroneously placed into the simulated rock matrix, but are actively migrating through low-velocity segments of the hydraulic backbone. The fact that the release area is in a fixed locale means that a large number of particles are placed into fractures with very low velocities that would not receive as much flux off of the backbone. Though solute particles are transported exclusively by advection in the numerical simulations, the movement of particles inside low-velocity fractures is very slow compared to the "mobile" portion of the plume.

[23] To characterize particle retention, we first consider the number of particles remaining in the source area, and then we analyze the velocity of particles that have moved outside the source area. The total number of particles in the source area exhibits power law decay (Figure 6a). Values of γ_1, the power law index, are in the range of $0.10 \leq \gamma_1 \leq 0.95$, although decay rates for the majority of network types fall within the range, $0.10 \leq \gamma_1 \leq 0.50$ (Table 1). Values of γ_1 for the upper endpoint (0.95) correspond to very dense networks dominated by short fractures (sets 12 and 14). With the exception of higher γ_1 values for the densest network end-members, values of γ_1 do not appear to reflect network type and decay rates are not always constant as multiple slopes are observed in some plots; however, these values indicate that solute retention occurs for all network types. We conclude that any transport model for fracture networks should include retention.

[24] The inverse of particle velocity ($1/v$) is commonly used as a measure of "residence time" of slow particles. The distribution of inverse velocity can be fit to a probability distribution which can then be represented as a memory function in a continuous time random walk (CTRW) [*Berkowitz and Scher*, 1997; *Painter et al.*, 2002; *Scher et al.*, 2002] or similar model of particle retention [*Schumer et al.*, 2003b; *Baeumer et al.*, 2005]. In our case, we analyze the distribution of inverse velocity for particles outside the source area. With the exception of sets 12 and 14 (dense networks with short fracture lengths), the largest residence time values, $1/v$ exhibit power law decay over several orders of magnitude (Figure 6b). The slope of the power law trend, γ_2 is equal to or near 1.0 for all time steps tested (Table 1). The presence of power law distributions of $1/v$ for the majority of our simulations are similar to the findings of *Painter et al.* [2002] and *Meerschaert and Scheffler* [2003] where power law distributions ($1.1 \leq \gamma \leq 1.8$) of both $1/v$ and $1/bv$ were found in discrete fracture network simulations with lognormal (finite variance) distri-

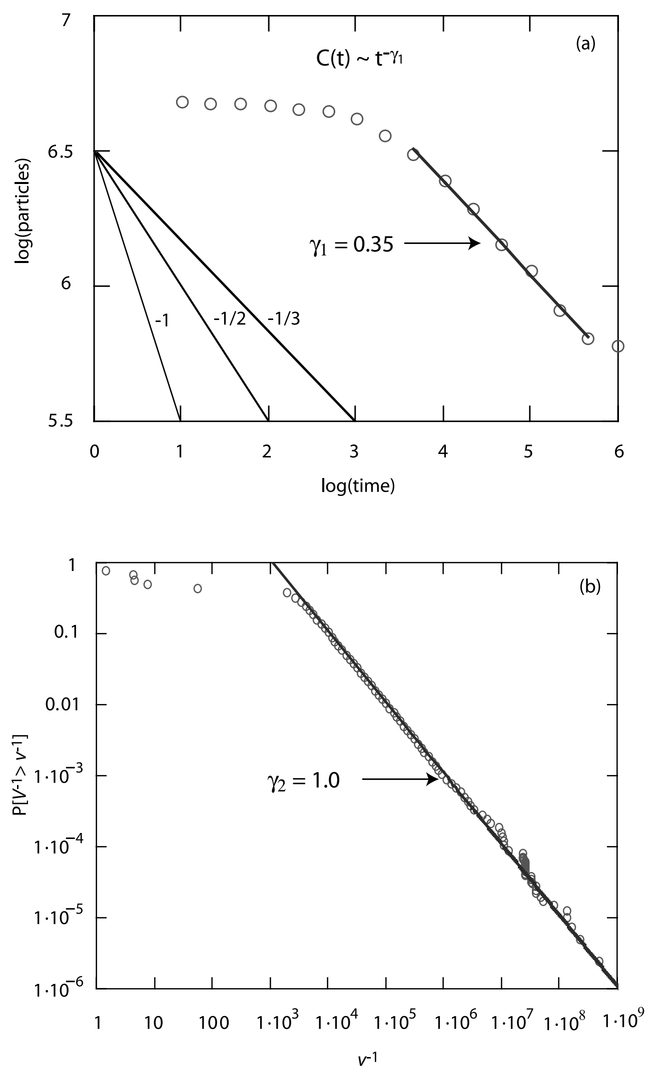

Figure 6. Slow particle transport is characterized by (a) power law decay of particles remaining in the source area where concentration at the source for a given time, $C(t)$, is proportional to $t^{-\gamma_1}$ and (b) power law residence time distributions of $1/v$. Values of γ describe the slope of the power law trends.

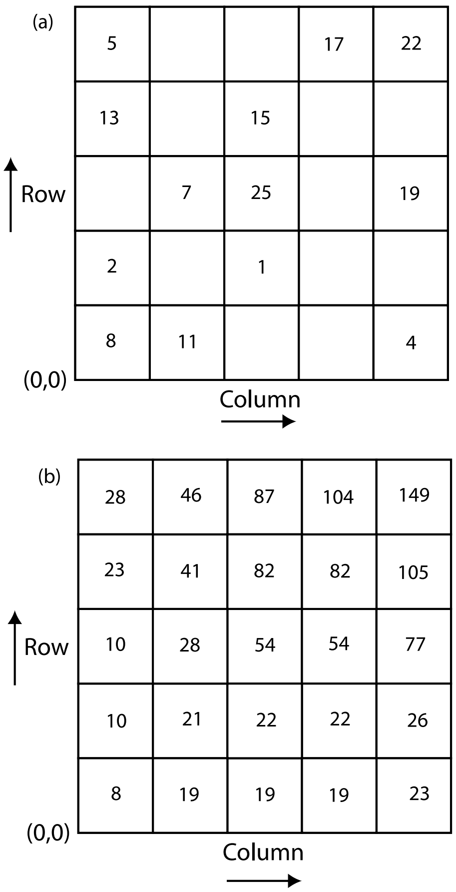

Figure 7. Computation of a bivariate CDF is similar to its univariate analog. (a) Number of particles per cell is adjusted to reflect (b) a cumulative particle total where the cumulative number of particles per cell increases in response to its row and column position on the grid. A bivariate CDF is obtained by dividing the cumulative number of particles in Figure 7b by the total number of particles (in this case 149).

butions of fracture length and aperture (b). The largest values of inverse velocity for sets 12 and 14 did not follow a power law, indicating that slow particle movement outside the release area is less prevalent for these two networks.

[25] Enhanced retention in the source area can be attributed to preferential paths. In the absence of mechanisms that promote solute mixing across streamlines, streamline routing at fracture intersections causes particles originally located in low-velocity segments in the source region to preferentially move into higher-velocity fractures. Once out of the source region, particles tend to stay in higher-velocity segments. Values of γ_2 may measure the influence of low-velocity segments which serve as critical links between higher-velocity segments. With the exception of the densest networks with short fractures (sets 12 and 14) where solute particles experienced the least amount of retention, our results indicate no clear relation between retention and fracture network statistics.

4. Ergodicity and Concentration Field Variability

[26] The purpose of this paper is to link ensemble plume statistics to quantifiable properties of a fractured medium, in order to inform waste repository design. For each set of fracture statistics, 500 fracture network realizations were produced, and the statistical analysis of the resulting ensemble plume, combining all of those particle plumes, was the subject of the previous section. In this section, we consider the important question of ergodicity: How closely do the individual plumes resemble their ensemble average? If deviations between ensemble and individual plumes are sufficiently small, ergodic conditions are present, and plume statistics computed from ensemble averages are useful for predicting individual plume behavior [*Black and Freyberg*, 1987; *Neuman et al.*, 1987; *Dagan*, 1989, 1990; *Graham and McLaughlin*, 1989; *Gelhar*, 1993]. Conversely, if deviations between ensemble and individual plume realizations are significant, solute transport predictions based on ensemble statistics are tenuous. With the exception of *Follin and Thunvik* [1994], who found that ergodic conditions were not achieved in a continuum model of highly heterogeneous crystalline rocks, the validity of the ergodic hypothesis for transport in fractured media has not been extensively tested.

[27] Although ergodicity in solute transport studies is traditionally defined according to spatial plume moments [*Black and Freyberg*, 1987; *Neuman et al.*, 1987; *Dagan*, 1989, 1990; *Graham and McLaughlin*, 1989; *Gelhar*, 1993], an analysis of ergodicity based on spatial moments is inappropriate for our data for several reasons. First, *Reeves et al.* [2008b] demonstrate that heavy tailed distributions of fracture trace length can lead to heavy tailed distributions of particle jumps, where the observed second moment of plume growth is not a reliable predictor of spread [*McCulloch*, 1997]. Second, the formation of immobile zones in low-velocity fractures results in particle retention near the source area, which distorts the moment estimates. Third, power law fracture length distributions do not have a "characteristic" fracture length. Instead, we use Kolmogorov distance to provide a nonparametric measure of variability between ensemble particle plumes and individual particle plume realizations [*Conover*, 1999]:

$$D(F,G) = \max\left|F(\vec{X}) - G(\vec{Y})\right| \tag{2}$$

where $D(F,G)$ represents the largest distance between cumulative distribution functions $F(\vec{X})$ for the ensemble and $G(\vec{Y})$ for individual particle plumes. The nonparametric Kolmogorov distance is valid for any distribution, including those with power law heavy tails. Particle jumps represent random displacement vectors in 2-D networks so that $F(\vec{X})$ and $G(\vec{Y})$ are bivariate CDFs. The bivariate CDF $F(\vec{X})$ counts the fraction of particles in a rectangle with $\vec{X}$ defining the upper right-hand corner. The computation of a bivariate CDF is similar to its univariate analog (Figure 7). To simplify computation, cells of the original domain (1 m by 1 m by 1 m) are combined into larger cells (50 m by 50 m by 1 m). A sensitivity analysis showed that a smaller cell size (10 m by 10 m by 1 m) did not significantly affect the Kolmogorov distance. Comparisons were made between all ensemble and individual plumes for each parameter set. The number of comparisons between individual and ensemble plumes are not equal, as some network types may not contain segments of a hydraulic backbone in the particle release area. The number of

Table 2. Kolmogorov Distance Statistics

Set	a_1[a]	a_2	ρ_{2D}[b]	μ	σ^2	Range
1	1.0	1.0	0.015	0.75	0.03	0.65
2	1.0	1.0	0.035	0.68	0.03	0.79
3	1.3	1.0	0.013	0.77	0.03	0.63
4	1.0	1.6	0.17	0.74	0.03	0.69
5	1.3	1.9	0.16	0.61	0.02	0.77
6	1.6	2.2	0.22	0.58	0.02	0.81
7	1.9	1.9	0.20	0.57	0.03	0.75
8	1.9	1.9	0.20	0.61	0.03	0.77
9	1.9	2.2	0.35	0.45	0.02	0.75
10	1.9	2.5	0.33	0.47	0.02	0.76
11	2.5	2.8	0.27	0.49	0.02	0.76
12	2.5	2.8	0.48	0.33	0.02	0.78
13	2.8	3.0	0.30	0.48	0.02	0.78
14	2.8	3.0	0.40	0.31	0.02	0.70
15	3.0	2.8	0.50	0.24	0.01	0.69

[a]Power law fracture length exponent.
[b]Average spatial fracture density value in model domain (m/m^2).

individual plume realizations for each parameter set ranges between 189 to 500; hence, no transport occurred at all for some realizations.

[28] To study the distribution of Kolmogorov distance for each parameter set, the minimum, maximum, range equals maximum minus minimum, mean (μ), and standard deviation (σ) of $D(F,G)$ was computed for each of 16 time steps. Table 2 lists these values for the time step with the largest values of μ. Data used to compute $F(\vec{X})$ and $G(\vec{Y})$ become censored at later time steps, when particles leave the model domain, and can no longer be tracked. One approach to data censoring would be to preserve the location where particles leave the model domain. Unfortunately, these locations were not recorded for these simulations. Censoring does not affect the results reported here, since the largest values of $D(F,G)$ (for the time steps tested) occur near the source area, where particle concentrations are highest because of retention in low-velocity fractures (e.g., Figures 8 and 9). Since Kolmogorov distance weights each particle equally, it is most sensitive to deviations in the area of highest concentration.

[29] By selecting the maximum value of the mean Kolmogorov distance, μ, between individual realizations and their ensemble average (out of 16 time steps) for each network type, a trend emerges between network type and the degree of variability between ensemble plumes and individual plume realizations (Figure 10). In general, values of μ for each parameter set are largest for sets 1–5 ($0.61 \leq \mu \leq 0.77$), intermediate for sets 6–10 ($0.45 \leq \mu \leq 0.61$), and smallest for sets 11–15 ($0.24 \leq \mu \leq 0.49$). More specifically, values of μ confirm that the higher the fracture length exponent (shorter fracture lengths) and spatial density, the less "heterogeneous" a fractured medium becomes. Since Kolmogorov distance is not commonly used to study concentration, we provide two examples of ensemble plumes along with several individual plume realizations and corresponding values of $D(F,G)$ for visual inspection (Figures 8 and 9). Individual plume realizations are based on values of $D(F, G)$ and correspond to minimum, maximum, and quantiles, $Q_{0.25}$, $Q_{0.50}$ and $Q_{0.75}$. The two network types (sets 5 and 15) represent the two end-members of our analysis. Set 5 is the network type with the highest degree

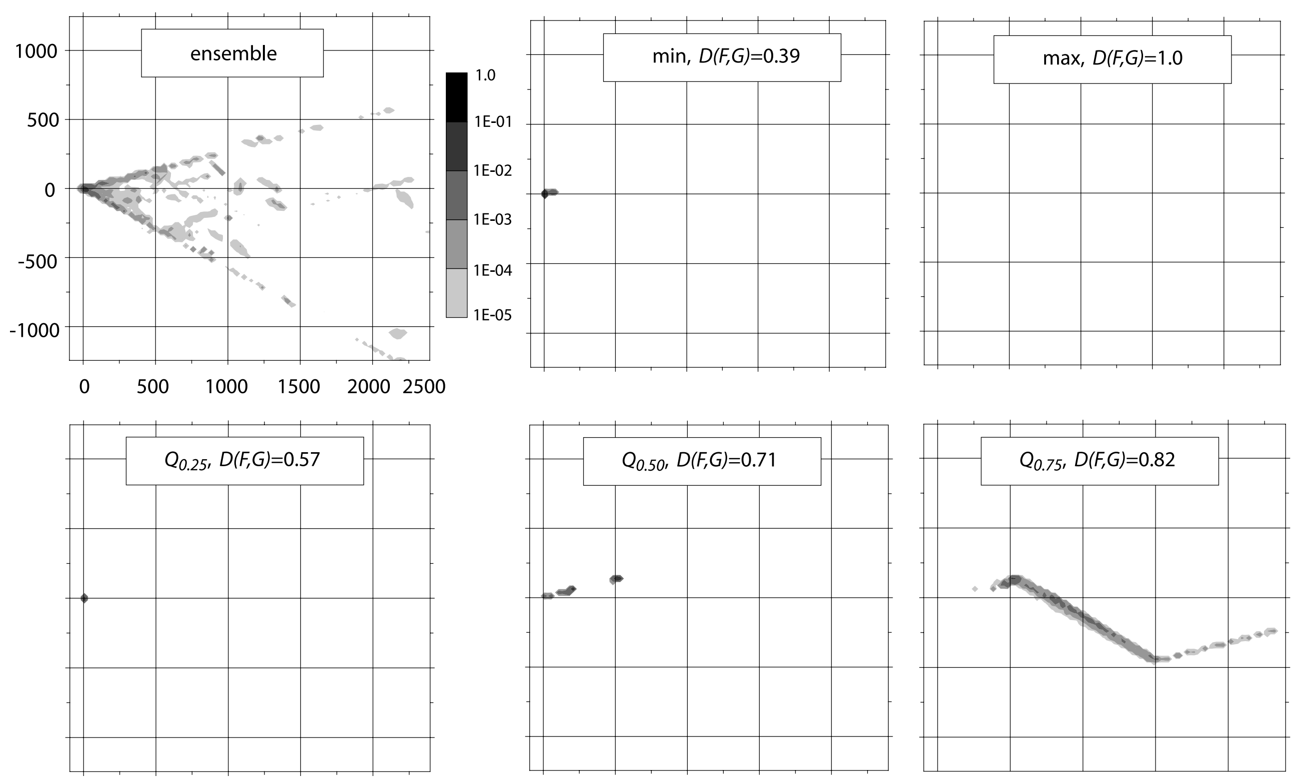

Figure 8. Ensemble plumes with selected individual plume realizations for set 5 at a transport time of 100 years. Sparse domains dominated by long fractures lead to a high degree of variability between ensemble and individual plumes. All particles have left the domain for the plume realization representing the maximum deviation from the ensemble. All spatial values are in units of meters.

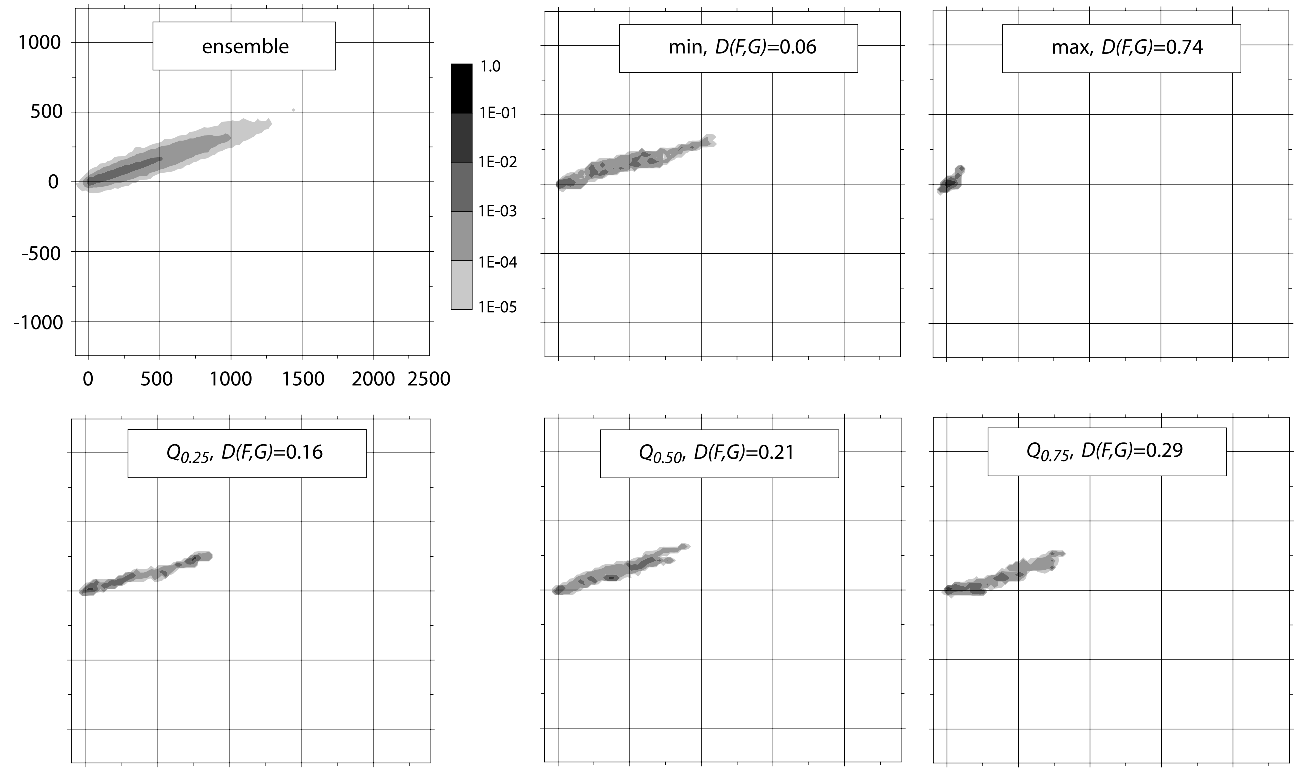

Figure 9. Ensemble plumes with selected individual plume realizations for set 15 at a transport time of 1000 years. Dense networks with short fractures lead to a lower degree of variability between ensemble and individual plumes. All spatial values are in units of meters.

of variability between ensemble and individual plume realizations (Figure 8). The fracture length combination (a_1 = 1.3, a_2 = 1.9) and low spatial density results in extremely low predictability from one realization to the next. In fact, the realization representing the maximum $D(F,G)$ for set 5 is a simulation where all particles have already left the domain by a transport time of 100 years. The dominance of short fractures and high density in set 15 results in fracture networks with the lowest degree of variability between individual realizations and the ensemble. The individual plume realizations exhibit nearly elliptical shapes (Figure 9).

[30] The standard deviation of $D(F,G)$ follows a similar trend as μ, but was not found to be a useful metric. The range of $D(F,G)$ is similar for all parameter sets indicating that large deviations occur between individual realizations and the ensemble for all network types. The large range in individual values of $D(F,G)$ demonstrate that ensemble particle motions in all networks of this study are pre-ergodic. Two primary explanations may account for the pre-ergodic nature of these plumes: the presence of particle retention at the source area limits the motion of a subset of particles (required for the fulfillment of mathematical limit theorems) and heavy tailed plumes in fractured media are highly variable. The first explanation is supported by *Margolin and Barkai* [2005] where significant deviations occurred between individual realizations and the ensemble of a heavy tailed retention (CTRW) process. A third possible explanation may be the result of the mixing assumption used in the particle-tracking simulations. At cells where fractures intersect, RWHet (E. M. LaBolle, RWHet: Random walk particle model for simulating transport in heterogeneous permeable media, version 2.0 user's manual and program documentation, 2000) computes particle trajectories on the basis of streamline routing (i.e., bilinear interpolation of the velocity field). The lack of solute particle mixing at fracture intersections reduces the number of flow paths sampled by particles, thus, increasing interrealization variability. This suggests that the selection

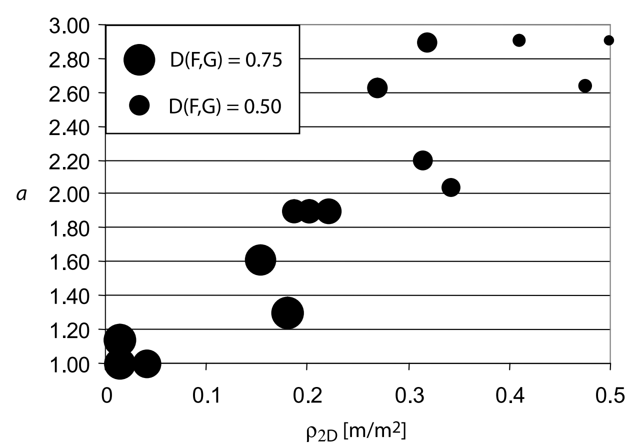

Figure 10. Mean Kolmogorov distance (proportional to size of dots) in relation to mean fracture length exponent a and spatial density ρ_{2D}. Note that mean Kolmogorov distance decreases as mean fracture length exponent and density increase.

of a mixing assumption may be more important than previously thought [e.g., *Park et al.*, 2001].

[31] As indicated by ballistic rates of plume growth (α is near 1.0) [*Mercado*, 1967], solute particles in individual realizations of sparsely fractured networks with relatively long fractures experience very little mixing between fracture flow paths. It is interesting that these individual plume realizations combine in the ensemble to resemble an operator-stable plume, the solution to a multiscaling fractional ADE, even though the individual plumes are much more irregular and unpredictable. For denser networks of shorter fractures, much less variability is observed between individual and ensemble plumes. Though pre-ergodic, mean values of Kolmogorov distance near 0.30 describe a medium where individual realizations are reasonably similar to the ensemble (e.g., Figure 9). Further development of stochastic theories based on realistic heavy tailed statistics are vital to characterize the between-realization variability more completely [*Berkowitz and Scher*, 1997; *Scher et al.*, 2002; *Schumer et al.*, 2003b; *Baeumer et al.*, 2005; *Bijeljic and Blunt*, 2006; *Le Borgne et al.*, 2007]. The lack of ergodicity for all fracture network types demonstrates that additional information on deterministic features of a fractured rock mass is useful to condition predictions of solute plume concentrations on the basis of ADEs. Classical and fractional-order ADEs, which model the ergodic limit, cannot account for the variability shown in individual realizations. However, those analytical equations remain useful for fractured media studies, as a way to characterize ensemble plume behavior, or the overall average risk of contamination at a preliminary phase, before detailed geologic information is available. This can be particularly useful for designing a monitoring well network for a geologic repository, where contours of either an operator-stable or multi-Gaussian density denote the likelihood of encountering a contaminant release. Uncertainty within these densities can be reduced through the identification and placement of monitoring wells on major deterministic structures.

5. Rock Mass Statistics and Geologic Repositories

[32] Geologic repositories designed for long-term storage of nuclear waste generally incorporate a dual barrier approach for waste containment that consists of an engineered component (waste form, canisters, backfill) and a geological component (rock mass and its geochemical, hydraulic, and structural properties) [e.g., *Long and Ewing*, 2004; *Research, Design and Development Programme*, 2004]. We adopt a contaminant transport perspective to identify fracture network statistics that are more favorable for a geologic repository. We evaluate (1) the probability that a solute particle enters the hydraulic backbone ($P(A)$), (2) the probability that a solute particle in the hydraulic backbone will undergo large transport distances within a repository timescale ($P(B|A)$), (3) the tendency for fast particle transport (α; t_{1km}), (4) the degree of particle retention in a network (γ), and (5) between-realization variability (Kolmogorov distance). The first four criteria of this analysis were presented in section 3.0, while the last criterion was presented in section 4.0. For ease of comparison, $P(A)$ and $P(B|A)$ are combined into the joint probability, $P(AB)$ (Table 1). $P(AB)$ defines the probability that a solute particle will both enter a hydraulic backbone and experience a displacement of at least 1 km in 10,000 years. Other geologic repository criteria are not considered [e.g., *National Research Council*, 1978; *Ewing et al.*, 1999].

[33] Currently, rock masses with moderate fracture lengths and densities just above the percolation threshold (similar to sets 5–8) are being evaluated for their potential as geologic repositories (e.g., Åspö Hard Rock Laboratory, Yucca Mountain). This network type selection is based on the principle that fractures serve as preferential pathways for fluids and solute in an otherwise impermeable rock matrix; fewer fracture pathways are thought to decrease the chance of contaminant transport. Values of $P(AB)$ on the order of 10^{-4} to 10^{-5} indicate that solute particles traveling through networks near the percolation threshold (sets 3, 4, 11 and 13) are least likely to exit a repository rock mass and enter the biosphere. For these network types, the hydraulic backbone is sparse and contains very few backbone cells in the particle release area (i.e., $P(AB)$ is dominated by $P(A)$). Longer fracture lengths for sets 3 and 4 result in a more sparse backbone than for sets 11 and 13. This is indicated by a lower probability of a particle entering the hydraulic backbone for sets 3 and 4 ($P(A) = 10^{-3}$) than for sets 11 and 13 ($P(A) = 10^{-2}$). Sparse backbones may also potentially lead to enhanced particle retention. If a solute particle is introduced into a low-velocity segment, large distances between the intersection of a low-velocity segment and a higher-velocity segment may isolate the particle from the rest of the plume. Though a trend between values of γ and network statistics was not found, this may partially explain why some networks have different rates of power law decay of particles from the source area. Outside of the source area, waiting time distributions between particle jumps are consistent for all networks (except sets 12 and 14).

[34] The primary difference between sets 3 and 4 and sets 11 and 13 is the distribution of fracture length. Longer fracture lengths for sets 3 and 4 lead to heavy tail leading plume edges, near ballistic transport rates (α is near 1.0) along primary plume growth directions, and a high tendency for very fast transport ($t_{1km} \leq 2.2$ years). For sets 11 and 13, the combination of very short fractures and densities just above the percolation threshold result in elliptical plumes with thin-tailed leading plume edges and very slow transport rates (t_{1km} values are 2154 and 10,000 years, respectively). Additionally, the influence of very long fracture lengths in sets 3 and 4 result in extreme variability between individual realizations and the ensemble (mean Kolmogorov distance is $\geq$0.7), where shorter fracture lengths in sets 11 and 13 promote moderate variability between the ensemble and individual realizations (mean Kolmogorov distance is $\approx$0.5). Overall, sets 11 and 13 indicate that the combination of short fracture lengths and densities near the percolation threshold are most suitable for geologic repositories, because this set of statistics promotes slow overall transport ($P(B|A) = 10^{-2}$ to 10^{-4}; $2150 \leq t_{1km} \leq 10{,}000$) and moderate predictability (mean Kolmogorov distance is approximately 0.5).

[35] Though sets 11 and 13 represent the best set of statistics for a geologic repository, more densely fractured domains with the same distributions of fracture length (sets 9, 12, and 14–15) are much less desirable. If a rock mass is fractured well beyond the percolation threshold, the probability of a solute particle entering the biosphere is very high

($P(AB) = 10^{-1}$). Aside from a high probability that solute particles will enter the hydraulic backbone exist, once in the backbone, higher densities result in both a decrease in the degree of transverse plume spreading [*Reeves et al.*, 2008b] and decreased retention times for particles in the source area. While fast particle transport times for these dense networks are intermediate ($100 \leq t_{1km} \leq 464$), the probability of a solute particle in the backbone experiencing a net displacement of at least 1 km within 10,000 years is extremely high ($P(B) \geq 0.7$). A positive aspect of the combination of high fracture densities and short fracture lengths is that particle motion in these networks exhibit low between-realization variability and higher levels of predictability. In contrast, chances of detecting a contaminant in networks with long fracture lengths (regardless of density) are very low, as the motion of particles in these networks is inherently unpredictable. Field-scale flow and transport studies in highly fractured rock masses are needed to validate these conclusions.

[36] **Acknowledgments.** This research was sponsored by grant DE-FG-02-07ER5841 from the Chemical Sciences, Geosciences, and Biosciences Division, Office of Basic Energy Sciences, Office of Science, U.S. Department of Energy, and by NSF grants DMS-0539176, DMS-0139943, DMS-0139927, DMS-0417869, DMS-0706440, and EAR-9980489; Desert Research Institute G.B. Maxey and NSF EPSCoR ACES fellowships; and the Marsden Fund, administered by the Royal Society of New Zealand. The DRI ACES supercomputer was essential for the numerical component of this research. The authors would like to acknowledge the inspiring discussions at the Working Group meeting ''Stochastic Transport and Emergent Scaling on Earth's Surface'' in Lake Tahoe, November 2007. This working group was sponsored by NCED (National Center for Earth-surface Dynamics), an NSF Science and Technology Center funded under contract EAR-0120914, and the Hydrologic Synthesis Activities at the University of Illinois funded by NSF under contract EAR-0636043.

References

Baeumer, B., D. A. Benson, and M. M. Meerschaert (2005), Advection and dispersion in time and space, *Physica A*, *350*(2–4), 245–262.

Benson, D. A., S. W. Wheatcraft, and M. M. Meerschaert (2000), Application of a fractional advection-dispersion equation, *Water Resour. Res.*, *36*(6), 1403–1412.

Berkowitz, B., and H. Scher (1996), Influence of embedded fractures on contaminant diffusion in geological formations, *Geophys. Res. Lett.*, *23*(9), 925–928.

Berkowitz, B., and H. Scher (1997), Anomalous transport in random fracture networks, *Phys. Rev. Lett.*, *79*(20), 4038–4041.

Bhattacharya, R., and V. K. Gupta (1990), Application of central limit theorems to solute transport in saturated porous media: From kinetic to field scales, in *Dynamics of Fluids in Hierarchical Porous Media*, edited by J. Cushman, pp. 61–96, Academic, London.

Bijeljic, B., and M. J. Blunt (2006), Pore-scale modeling and continuous time random walk analysis of dispersion in porous media, *Water Resour. Res.*, *42*, W01202, doi:10.1029/2005WR004578.

Black, T. C., and D. L. Freyberg (1987), Stochastic modeling of vertically averaged concentration uncertainty in a perfectly stratified aquifer, *Water Resour. Res.*, *23*(6), 997–1004.

Bonnet, E., O. Bour, N. E. Odling, P. Davy, I. Main, P. Cowie, and B. Berkowitz (2001), Scaling of fracture systems in geologic media, *Rev. Geophys.*, *39*(3), 347–383.

Brooks, B. A., R. W. Allmendinger, and G. I. de al Barra (1996), Fault spacing in the El Teniente Mine, central Chile: Evidence of nonfractal fault geometry, *J. Geophys. Res.*, *101*(B6), 13,633–13,653.

Conover, W. J. (1999), *Practical Nonparametric Statistics*, John Wiley, New York.

Dagan, G. (1989), *Flow and Transport in Porous Media Formations*, Springer, Berlin.

Dagan, G. (1990), Transport in heterogeneous porous formations: Spatial moments, ergodicity, and effective disperison, *Water Resour. Res.*, *26*(6), 1281–1290.

Davy, P. (1993), On the frequency-length distribution of the San Andreas fault system, *J. Geophys. Res.*, *98*(B7), 12,141–12,151.

Ewing, R. C., M. S. Tierney, L. F. Konikow, and R. P. Rechard (1999), Performance assessments of nuclear waste repositories: A dialogue on their value and limitations, *Risk Anal.*, *19*(5), 933–958.

Follin, S., and R. Thunvik (1994), On the use of continuum approximations for regional modeling of groundwater flow through crystalline rocks, *Adv. Water Resour.*, *17*, 133–145.

Gelhar, L. W. (1993), *Subsurface Stochastic Hydrology*, Prentice-Hall, Englewood Cliffs, N. J.

Graham, W., and D. McLaughlin (1989), Stochastic analysis of nonstationary subsurface solute transport: 1. Unconditional Moments, *Water Resour. Res.*, *25*(2), 215–232.

Gustafson, G., and A. Fransson (2005), The use of the Pareto distribution for fracture transmissivity assessment, *Hydrogeol. J.*, *14*, 15–20, doi:10.1007/s10040-005-0440-y.

Jurek, Z., and J. D. Mason (1993), *Operator-Limit Distributions in Probability Theory*, John Wiley, New York.

Kozubowski, T. J., M. M. Meerschaert, and G. Gustafson (2008), A new stochastic model for fracture transmissivity assessment, *Water Resour. Res.*, *44*, W02435, doi:10.1029/2007WR006053.

LeBorgne, T., J.-R. de Dreuzy, P. Davy, and O. Bour (2007), Characterization of the velocity field organization in heterogeneous media by conditional correlation, *Water Resour. Res.*, *43*, W02419, doi:10.1029/2006WR004875.

Long, J. C. S., and R. C. Ewing (2004), Yucca Mountain: Earth-science issues at a geologic repository for high-level nuclear waste, *Annu. Rev. Earth Planet Sci.*, *32*, 363–401, doi:10.1146/annurev.earth.32.092203.122444.

Margolin, G., and E. Barkai (2005), Nonergodicity of blinking nanocrystals and other Levy-walk processes, *Phys. Rev. Lett.*, *94*, 080601, doi:10.1103/physRevLett.94080601.

McCulloch, J. H. (1997), Measuring tail thickness to estimate the stable index α: A critique, *J. Bus. Econ. Stat.*, *15*, 74–81.

McDonald, M. G., and A. W. Harbaugh (1988), A modular three-dimensional finite-difference ground-water flow model, *U. S. Geol. Surv. Tech. Water Resour. Invest.*, *Book 6, Chap. 2*.

Meerschaert, M. M., and H. P. Scheffler (2001), *Limit Distributions for Sums of Independent Random Vectors: Heavy Tails in Theory and Practice*, John Wiley, New York.

Meerschaert, M. M., and H. P. Scheffler (2003), Nonparametric methods for heavy tailed vector data: A survey with applications from finance and hydrology, in *Recent Advances and Trends in Nonparametric Statistics*, edited by M. G. Akritas and D. N. Politis, pp. 265–279, Elsevier Sci., Amsterdam.

Meerschaert, M. M., D. A. Benson, and B. Baeumer (2001), Operator Lévy motion and multiscaling anomalous diffusion, *Phys. Rev. E*, *63*, 021112.

Mercado, A. (1967), The spreading pattern of injected water in a permeability-statified aquifer, *IAHS AISH Publ.*, *72*, 23–36.

National Research Council (1978), *Geological Criteria for Repositories for High-Level Radioactive Wastes*, Natl. Acad., Washington, D. C.

National Research Council (1996), *Rock Fractures and Fluid Flow: Contemporary Understanding and Applications*, Natl. Acad., Washington, D. C.

Neuman, S. P. (2005), Trends, prospects and challenges in quantifying flow and transport through fractured rocks, *Hydrogeol. J.*, *13*, 124–147.

Neuman, S. P., C. L. Winter, and C. M. Neuman (1987), Stochastic theory of field scale dispersion in anisotropic porous media, *Water Resour. Res.*, *23*(3), 453–466.

Painter, S., and V. Cvetkovic (2005), Upscaling discrete fracture network simulations: An alternative to continuum transport models, *Water Resour. Res.*, *41*, W02002, doi:10.1029/2004WR003682.

Painter, S., V. Cvetkovic, and J. Selroos (2002), Power-law velocity distributions in fracture networks: Numerical evidence and implications for tracer transport, *Geophys. Res. Lett.*, *29*(14), 1676, doi:10.1029/2002GL014960.

Park, Y. J., J. R. De Dreuzy, K. K. Lee, and B. Berkowitz (2001), Transport and intersection mixing in random fracture neworks with power-law length distributions, *Water Resour. Res.*, *37*(11), 2493–2501.

Reeves, D. M., D. A. Benson, and M. M. Meerschaert (2008a), Transport of conservative solutes in simulated fracture networks: 1. Synthetic data generation, *Water Resour. Res.*, *44*, W05404, doi:10.1029/2007WR006069.

Reeves, D. M., D. A. Benson, M. M. Meerschaert, and H.-P. Scheffler (2008b), Transport of conservative solutes in simulated fracture networks: 2. Ensemble solute transport and the correspondence to operator-stable limit distributions, *Water Resour. Res.*, *44*, W05410, doi:10.1029/2008WR006858.

Renshaw, C. E. (1996), Influence of subcritical fracture growth on the connectivity of fracture networks, *Water Resour. Res.*, *32*(6), 1519–1530.
Renshaw, C. E. (1997), Mechanical controls on the spatial density of opening-mode networks, *Geology*, *25*(10), 923–926.
Renshaw, C. E. (1999), Connectivity of joint networks with power law length distributions, *Water Resour. Res.*, *35*(9), 2661–2670.
Research, Design and Development Programme (2004), Programme for research development and demonstration of methods for the management and disposal of nuclear waste, including social science research, *TR-04-21*, Swed. Nucl. Fuel and Waste Manage. Co., Stockholm.
Rives, T., M. Razack, J.-P. Petit, and K. D. Rawnsley (1992), Joint spacing: Analogue and numerical simulations, *J. Struct. Geol.*, *14*, 925–937.
Ross, S. M. (1985), *Introduction to Probability Models*, 3rd ed. Academic, Orlando, Fla.
Scher, H., G. Margolin, and B. Berkowitz (2002), Towards a unified framework for anomalous transport in heterogeneous media, *Chem. Phys.*, *284*, 349–359.
Schumer, R., D. A. Benson, M. M. Meerschaert, and B. Baeumer (2003a), Multiscaling fractional advection-dispersion equations and their solutions, *Water Resour. Res.*, *39*(1), 1022, doi:10.1029/2001WR001229.
Schumer, R., D. A. Benson, M. M. Meerschaert, and B. Baeumer (2003b), Fractal mobile/immobile solute transport, *Water Resour. Res.*, *39*(10), 1296, doi:10.1029/2003WR002141.
Schwartz, F. W., and L. Smith (1988), A continuum approach for modeling mass transport in fractured media, *Water Resour. Res.*, *24*(8), 1360–1372.
Wines, D. R., and P. A. Lilly (2002), Measurement and analysis of rock mass discontinuity spacing and frequency in part of the Fimiston Open Pit operation in Kalgoorlie, West Australia: A case study, *Int. J. Rock Mech. Min. Sci.*, *39*, 589–602.

D. A. Benson, Department of Geology and Geological Engineering, Colorado School of Mines, 1500 Illinois Street, Golden, CO 80401, USA. (dbenson@mines.edu)

M. M. Meerschaert, Department of Statistics and Probability, Michigan State University, A416 Wells Hall, East Lansing, MI 48824, USA. (mcubed@stt.msu.edu)

D. M. Reeves, Desert Research Institute, 2215 Raggio Parkway, Reno, NV 89512, USA. (mreeves@dri.edu)